Nonthermal plasma synthesis of aluminum nanoparticles

A THESIS
SUBMITTED TO THE FACULTY OF THE GRADUATE SCHOOL
OF THE UNIVERSITY OF MINNESOTA
BY

Benjamin Pearce

IN PARTIAL FULFILLMENT OF THE REQUIREMENTS
FOR THE DEGREE OF
MASTER OF SCIENCE

Uwe Kortshagen

August, 2017

Acknowledgements

There are many people I want to thank for their help and guidance during my time as a master's student.

First, I would like to express my gratitude to my advisor, Professor Uwe Kortshagen, for giving me the opportunity to work and learn in his lab. I also want to thank Ben Greenberg for being there whenever I needed advice as well as every other member of the Kortshagen group. You all helped make my time as a graduate student an enriching experience.

I would like to thank Bing Luo for his help in collecting XPS data from my samples as well as Jacob Held of the Mkhoyan Group at the University of Minnesota for collecting and interpreting the raw images and EDS data from my samples using the FEI Titan G2 60-300 STEM. Finally, I want to thank Javier Barriocanal and Seema Thakral for teaching me how to seal my aluminum nanoparticles in air-free sample holders for XRD data acquisition.

Parts of this work were carried out in the Characterization Facility, University of Minnesota, which receives partial support from NSF through the MRSEC program.

Dedication

To my parents, Mac & Anne, my sister, Laura, and my fiance, Anna.

Abstract

Aluminum nanoparticles are an intriguing material because of their high reactivity and high energy density, making them ideal for propellant materials such as rocket fuel. In addition, nanoaluminum is also a promising abundant, low cost material for plasmonic applications with a plasmonic response that can extend from the visible region of the light spectrum down to ultraviolet wavelengths of light. Nonthermal plasmas are a promising tool for synthesizing nanocrystalline materials without the need for high temperatures or solvents. Their ability to add electrons to the surface of nanoparticles within the plasma helps reduce agglomeration and form aerosols with tighter size distributions than other competing aerosol synthesis techniques.

Nanoparticles containing crystalline elemental aluminum were synthesized using a nonthermal plasma containing trimethylaluminum (TMA) vapor, argon and hydrogen gases. The percentage of hydrogen flowing with respect to total gas flow was required to be at least 70% in order to form crystalline aluminum. In addition the ratio of H_2 to TMA flow rates needed to be a minimum of 60. 7% of the nanoparticles' aluminum atoms were in elemental aluminum form with the remaining ones in the form of alumina (Al_2O_3) or an aluminum hydroxide according characterization by air-free X-ray photoelectron spectroscopy. Air-free X-ray diffraction of the nanoparticles indicated the average crystallite size of the elemental aluminum in the particles was on the other of a few nanometers.

Contents

List of Tables

List of Figures

Chapter 1

Introduction

1.1 Aluminum nanoparticles and plasmonics

Aluminum is the most abundant metal in the earth's crust [2]. As a nanomaterial it can be utilized in a plethora of applications, such hydrogen generation [3] [4], as a propellant in rocket fuel and as a photocatalyst in hydrogen dissociation [5].

The plasmonic properties of aluminum nanoparticles have generated interest. Expensive precious metals such as gold and silver can support resonances extending from 700nm down to 350nm. Aluminum's plasmonic resonance, however, can span from the visible range of light all the way down to ultraviolet wavelengths of around 200nm as seen in figure 1.1.

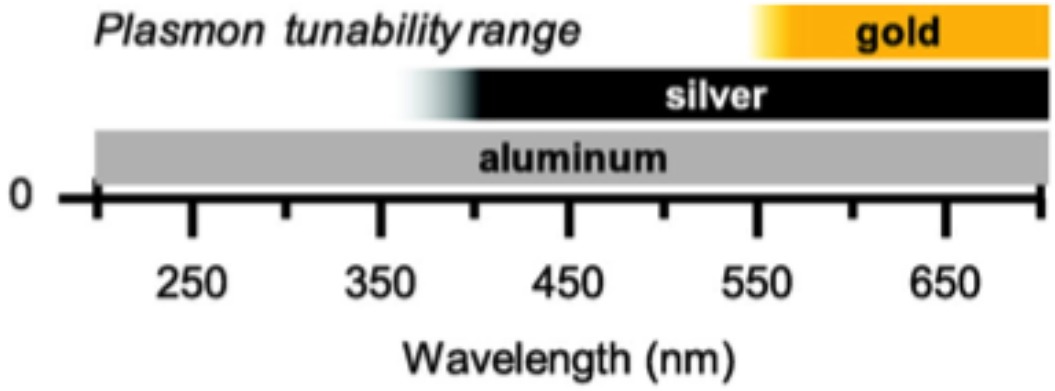

Figure 1.1: Aluminum's plasmonic tunability extends further into the UV than silver [1].

Knight *et. al* demonstrated this experimentally and using simulations to show how sensitive aluminum's plasmonic response is to the presence of an oxide layer. The more the amount of oxide increased in their 100 nm diameter Al disks, the further the plasmonic peak red-shifted (i.e. increased the wavelength) [1].

1.2 Overview of gas-phase nanoparticle aerosol generation methods

The gas-phase synthesis of nanoparticles can be broken down into two major categories: ones involving physical or chemical changes. Processes that utilize physical changes typically involve evaporating the material of interest from a solid into a vapor using heat or some other type of energy input. After the source material evaporates into the gas-phase, rapid quenching follows in which the substance cools and forms nanoparticles. Processes that utilize chemical changes involve delivery of a chemical vapor or aerosolized liquid precursor into a reactor zone where it then undergoes a chemical reaction upon addition of energy (e.g. with heat or electricity). The final product then condenses into solid nanoparticles.

A review by Swihart of nanoparticle synthesis in the gas-phase notes how the physical and chemical syntheses share a common feature [6]. Both involve establishing conditions such that the substance's gas phase is thermodynamically less favorable than the formation of solid nanoparticles. In the gas-phase once the vaporized substance achieves a high enough level of supersaturation coinciding with the appropriate condensation conditions, the particles begin forming through homogeneous nucleation, which alleviates the vapor supersaturation. Once enough of these initial particles are formed, additional vapor condenses on them, further reducing the amount of supersaturation.

He classified these syntheses based on the precursor's initial phase (e.g. solid, liquid or gas) and the energy input method used to create the supersaturated vapor that eventually forms nanoparticles.

1.2.1 Nanoparticle synthesis using solid precursors

Swihart reviewed a variety of methods used to create nanoparticles using solid precursors. These involve inert gas condensation, pulsed laser ablation and spark discharge

generation. In addition an atmospheric arc evaporation method used by Mahoney *et. al* has also been used to generate metal nanoparticles [7].

Inert gas condensation involves heating a solid precursor into a hot gas, then mixing it with a cool inert gas such as argon or a reactive one such as oxygen to form oxides. It is convenient for producing metal nanoparticles since they can evaporate quickly enough at feasible temperatures [6]. The average size of bismuth nanoparticles synthesized in this fashion could be controlled by tuning the carrier or quenching gas flow rates as well as processing pressure. Pulsed laser ablation provides a more targeted approach to vaporize solid material by using the laser to evaporate a small amount of solid material, which subsequently condenses from a supersaturated vapor state in a background gas into nanoparticles. One advantage of pulsed laser ablation over inert gas condensation is that it can vaporize materials that cannot be readily evaporated at relatively lower temperatures compared to pure metals, for example. On the other hand, this process produces smaller amounts of nanoparticles than inert gas condensation.

Spark discharge generation involves applying a voltage across a pair of metal electrodes in the presence of an inert gas until the breakdown voltage is reached, providing the energy required to vaporize those metal atoms. Metal oxides can be produced by using a reactive gas such as oxygen rather than an inert gas [6]. Schwyn *et. al* showed that one advantage of this process is that it can generate nanoparticles of any conductive material and charge those very nanoparticles, preventing agglomeration thanks to the electrical repulsion forces [8]. They also noted the addition of turbulent gas flow through a nozzle into the region of particle formation was necessary to form a monodisperse aerosol by diluting the number concentration of particles. Lowering the number density of nanoparticles is crucial for the formation of monodisperse aerosols. Otherwise coagulation, whose rate is proportional to the number concentration squared will occur and form a polydisperse aerosol. Like pulsed laser ablation, this method provides a relatively smaller amount of particles compared to other techniques.

Atmospheric arc evaporation involves generating a direct current (DC) arc discharge between two electrodes at atmospheric pressure. In the study presented by Mahoney *et. al* their upper electrode was made of tantalum, whereas a heavy gauge tungsten wire basket served as the lower electrode. Upon arc ignition, the tungsten wire's temperature rises quickly, causing the metal evaporant within the basket to become molten and

transition into the gas phase with rising temperature. As with inert gas evaporation, the gaseous metal was mixed in a quench region with a cooler inert gas such as argon. The quench gas served two purposes: to cool the metal vapor, promoting nanoparticle formation and to dilute nanoparticle concentration. Since agglomeration of particles is proportional to the square of number density, it must be suppressed if there is to be any control over particle size. The authors were able to achieve mean cluster diameters in the 1-100 nm range and also observed a reduction in mean particle size with a narrowing size distribution corresponding to increased quench flow rates. As with inert gas condensation their process could also produce metal oxides or metal nitrides by using reactive gases in the reactor's evaporation or quench region.

1.2.2 Nanoparticle synthesis using liquid or gaseous precursors

The solid precursor processes described in section 1.2.1 produce metal nanoparticles using physical changes. Liquid and gaseous precursors, on the other hand, form metal nanoparticles in the gas-phase via chemical reactions. A source of energy is required to break the chemical bonds containing the desired metal atoms. Once the metal atoms are finally liberated from the parent precursor in a supersaturated vapor, they subsequently undergo homogeneous nucleation to form nanoparticle clusters.

Synthesis methods involving liquid and vaporous precursors can be differentiated based on the source of energy used to decompose the compounds containing the metal atoms of interest. These techniques include methods such as chemical vapor synthesis, spray pyrolysis, thermal plasma synthesis and laser photolysis.

Chemical vapor condensation (CVC) or synthesis is a process that competes with chemical vapor deposition (CVD). CVD is a process used to deposit solid thin films on a target surface using a combination of gas-phase and surface reactions involving the precursor. The precursor can be a solid, liquid or gas at room temperature and atmospheric pressure, but is supplied to the reactor in vapor form [6]. This can be accomplished by using a bubbler, an atomizer to deliver liquid droplets of precursor into the reactor, or by sublimating a solid precursor. A major advantage of CVC is that this method is continuous, unlike batch processes. It can produce more than 20 g/hr of nanoparticles in a laboratory setting [9].

Nanoparticle formation is an undesired by-product that can occur due to homogeneous nucleation in the gas-phase. Kodas states that particle formation in CVD reactors can be reduced through lower pressures, shorter transport distance to the substrate upon which the film deposits and lowering the rates of homogeneous gas-phase reactions vs. heterogeneous (substrate surface) reactions as noted by Kodas and Smith [10]. Lower pressures increase the mean free path of chemical species in a CVD reactor, while also reducing the concentration of gaseous species. This suppresses the number of collisions the vaporous precursors encounter in order for them to reach the substrate and react there to form solid thin films. Hahn argues the crucial parameter for controlling nanoparticle vs. thin film formation is the residence time of precursor molecules [9].

An alternative to CVC is spray pyrolysis. In this method droplets of precursor are injected into the reaction zone using an atomizer rather than in vapor form. The precursor chemically dissociates due to the heat inside the reactor to produce a supersaturated vapor of metal atoms that finally nucleate to form nanoparticles.

Rather than heating a whole enclosed volume using high temperatures, a laser light can be used to chemically dissociate a small area of vaporous precursor. This process is called laser pyrolysis. Typically an infrared CO_2 laser is used heat the precursor [6].

1.3 Gas-phase synthesis of aluminum nanoparticles

A variety of gas-phase synthesis methods have been developed to synthesize aluminum nanoparticles. Many of the methods used to produce aluminum nanoparticles consist of processes discussed in section 1.2.

These include evaporation of molten Al in the presence of an inert gas [11], the exploding wire method [11], laser ablation [11], furnace synthesis [12], thermal plasmas [13, 14]

Triisobutylaluminum (TIBA) vapor has been used to synthesize faceted polyhedral and spherical aluminum nanocrystals in a series of two furnaces [12]. The temperature settings in the furnaces were below the melting of aluminum (660°C), but high enough to decompose TIBA.

Several types of thermal plasma synthesis techniques have been used to generate aluminum nanoparticles. In thermal plasmas the electron temperature is equal to that

of the ions and neutral species. The electrical energy transmitted into the plasma along with the additional heat helps decompose almost any type of precursor.

A study by Weigle et al. [15] involved passing micrometer-sized Al particles through an atmospheric pressure argon plasma torch. Another by Zhang [13] involved sending sublimated $AlCl_3$ into an Ar/H_2 plasma torch to generate ultrafine aluminum particles. One benefit to this approach is its continuous flow approach. Continuous gas-phase flow processes are advantageous because they can be scaled up easily from laboratory to industry. In addition this eliminates the need for wet solvents. They can be become expensive to use in manufacturing settings when dealing with liquid waste products etc [16].

On an industrial scale, thermal plasmas are less desirable because of the high cost required to heat and provide appropriate cooling around it. Nonthermal plasmas differ from their thermal counterpart because the electrons and ions are not in thermal equilibrium. The electrical power used to sustain nonthermal plasmas goes predominately into the kinetic energy of the relatively lighter electrons instead of ions or neutral gas molecules. This means the electrons are much hotter. This means nonthermal plasmas operate around room temperature unlike the studies cited above. Finally, this type of plasma is ubiquitous and its use is well-established in the semiconductor industry.

1.4 Nonthermal plasma synthesis of nanoparticles

Nonthermal plasmas have been used to produce a wide variety of nanomaterials and offer several advantages over other gas-phase processes as discussed by Kortshagen et al. [17]. They noted the electron temperature in these low pressure discharges can range from 10,000-50,000 K. Their high kinetic energy can break down and ionize precursor gas molecules, creating reactive ions and radicals. The dissociated precursor molecules can nucleate to form nanoparticles. Reactions on the surface of these particles due to the highly reactive ions and radicals inside the plasma can provide enough heat for crystallization. This eliminates the need for high temperatures required to crystallize them.

Finally Kortshagen *et. al* note that nanoparticles in nonthermal plasmas are usually

negatively charged, which prevents agglomeration. This results in narrow size distributions. In addition the walls of these types of reactors develop a negative voltage with respect to the plasma itself. This reduces diffusion loses due to the Brownian motion of these nanometer-sized particles compared to other aerosol reactors [17].

Chapter 2

Reactor design & overivew of characterization methods

2.1 Plasma Reactor Design

Aluminum nanoparticles were synthesized in a nonthermal, low-pressure, capacitively-coupled, radio-frequency (RF) (13.56MHz) plasma within a clearfused quartz tube. A diagram of the reactor can be seen in figure 2.1. The gases fed to the reaction zone of the quartz tube were argon (Ar), trimethylaluminum (TMA) and hydrogen (H_2) gas. TMA served as the aluminum precursor with hydrogen as the reduction agent, which is commonly used for this purpose in metal CVD [10]. Figure 2.1 shows a sketch of the reactor.

The tube's inner and outer diameters were 45mm and 48mm, respectively. A 13.56MHz AG 0313 power supply sold by T&C power conversion Inc. was used to supply energy needed to sustain the plasma discharge.

A custom built L-matching network consisting of an inductor and capacitor was used to maximize the power transfer from the power supply to the gas discharge. Two copper ring electrodes with a spacing of about 2.0 cm were used to deliver electrical power to sustain the gas discharge.

TMA vapor was delivered through a bubbler assembly using Ar as the carrier gas. All liquids are in a dynamic equillibrium between their vapor and liquid state, which means that a a given temperature, some of the liquid evaporates into vapor. A carrier

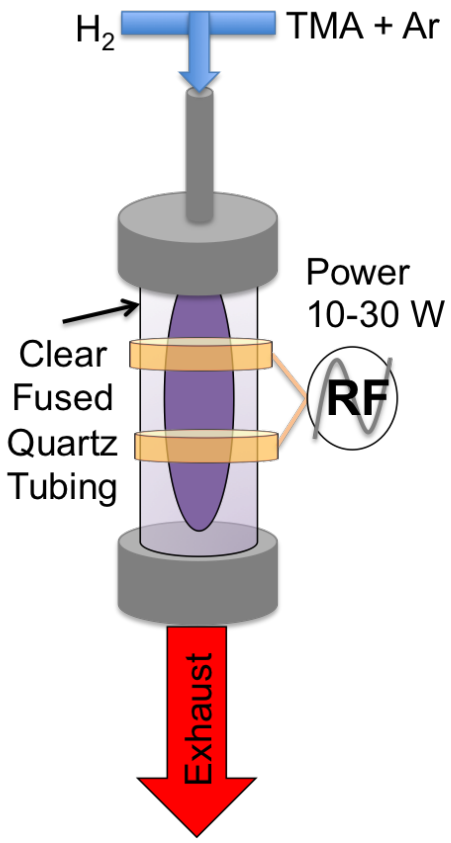

Figure 2.1: TMA was delivered to the Ar and/or H_2 plasma where it reacts to form nanoparticles which accelerate through an orifice and impact onto a downstream substrate.

gas such as argon is used to sweep it out of the bubbler and to the reactor.

A diagram of the reactor is shown in figure 2.2.

2.2 Brief Overview of Metal Precursors

The selection of an appropriate precursor is one of the most important steps for designing a gas-phase synthesis process. The range of suitable precursors is generally limited by the system's operating conditions (e.g. reactor temperature), which dictate the type of chemical reactions the precursor can undergo. These can result in the formation of the desired material as well as the formation of unintended byproducts. Ideally the

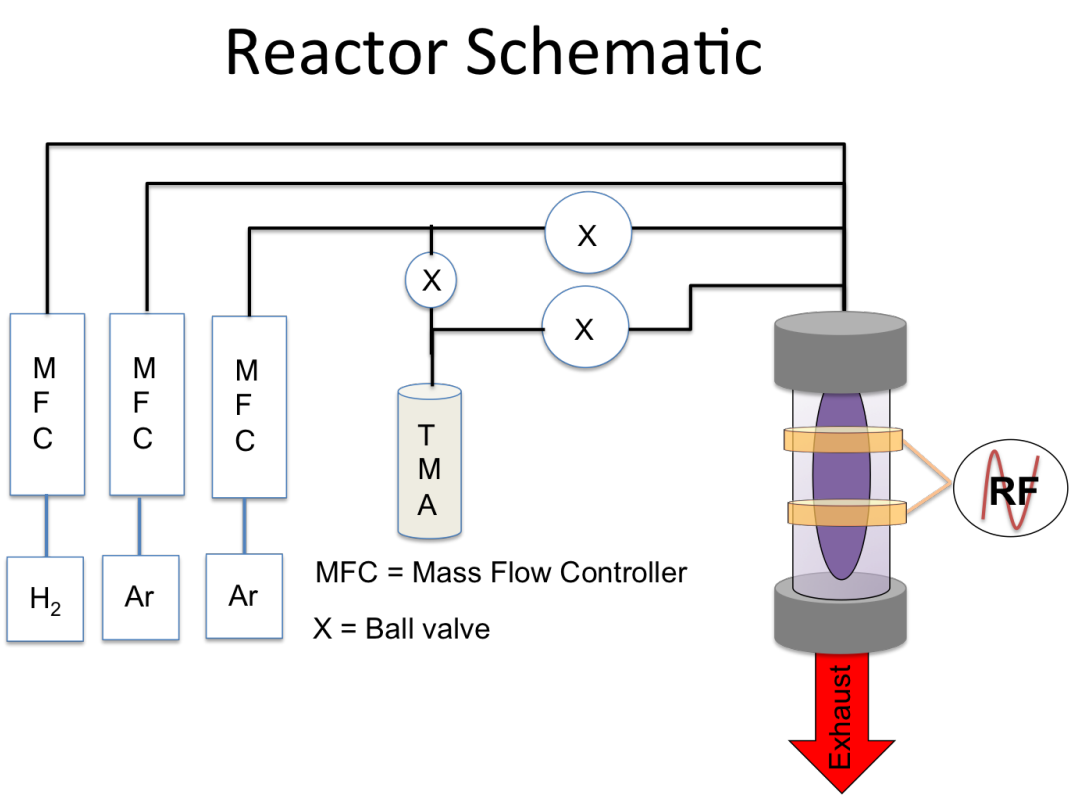

Figure 2.2: A schematic of the reactor shows how hydrogen was sent directly to the reactor along with dilution argon. When the bypass valve was open, carrier argon gas could flow direcly to the reactor. With the bypass valve shut and the bubbler valves open, carrier Ar was used to deliver TMA to the plasma.

chosen synthesis route should produce just the solid material of interest while any other substances are easily removed from the system. For example, a precursor can react to form the desired solid material and gaseous product(s) that are removed via the vacuum exhaust.

Metal precursors are categorized into three groups based on their chemical structure. They consist of inorganic (those without any carbon atoms), metal-organic (which contain organic ligands, but no metal-carbon bonds) and organometallic precursors, which feature metal-carbon bonds and have organic ligands [10]. A major source of concern in the deposition of high-purity metal thin films is incorporation of chemical impurities within the bulk of the material or on its surface.

Synthesizing pure metals using metal-organic and organometallic compounds can include the risk of unintentional carbon incorporation. To avoid this predicament a second reagent can be added to the reaction. Reducing agents such as hydrogen, H_2, are often applied to remove carbon impurities [10]. For example, if the organic ligand bonded to the metal atom is an alkyl group, then the leaving alkyl group can bond with a hydrogen atom to form a gaseous alkane such as methane or ethane.

2.3 Aluminum precursors

An example of a popular aluminum precursor is triisobutylaluminum (TIBA). It has been used as a CVD precursor to make high purity Al films since, but requires heating the lines in order to attain a appreciable vapor pressure.

A table of common aluminum precursors commonly used in Al CVD is shown in table 2.1

Table 2.1: **Common Aluminum Precursor Vapor Pressures**

Precursor (Abbreviation)	**Vapor Pressure (Torr)**[°C]
Trimethylaluminum (TMA)	11.0 (20)
Triethylaluminum (TEA)	0.1 (36)
Triisobutylaluminum (TIBA)	0.1 (27)
Diethylaluminumchloride (DEACl)	3.0 (60)
Trimethylamine alane (TMAA)	1.1 (19)
Triehtylamine alane (TEAA)	0.5 (36)
Dimethylethylamine alane (DMEAA)	1.5 (25)

Antoine equation plots of vapor pressure vs. temperature for trimethylaluminum, triethylaluminum and diethylaluminumchloride, listed in table 2.1, are shown in figure 2.3 [18].

Unfortunately, its vapor pressure is two orders of magnitude lower than TMA near room temperature. Feeding triisobutylaluminum into the reactor would require heating the bubbler as well the stainless steel tubing in order to have an appreciable flowrate of precursor and prevent condensation of the vapor in the lines. Similarly, other common aluminum precursors possess lower room-temperature vapor pressures compared

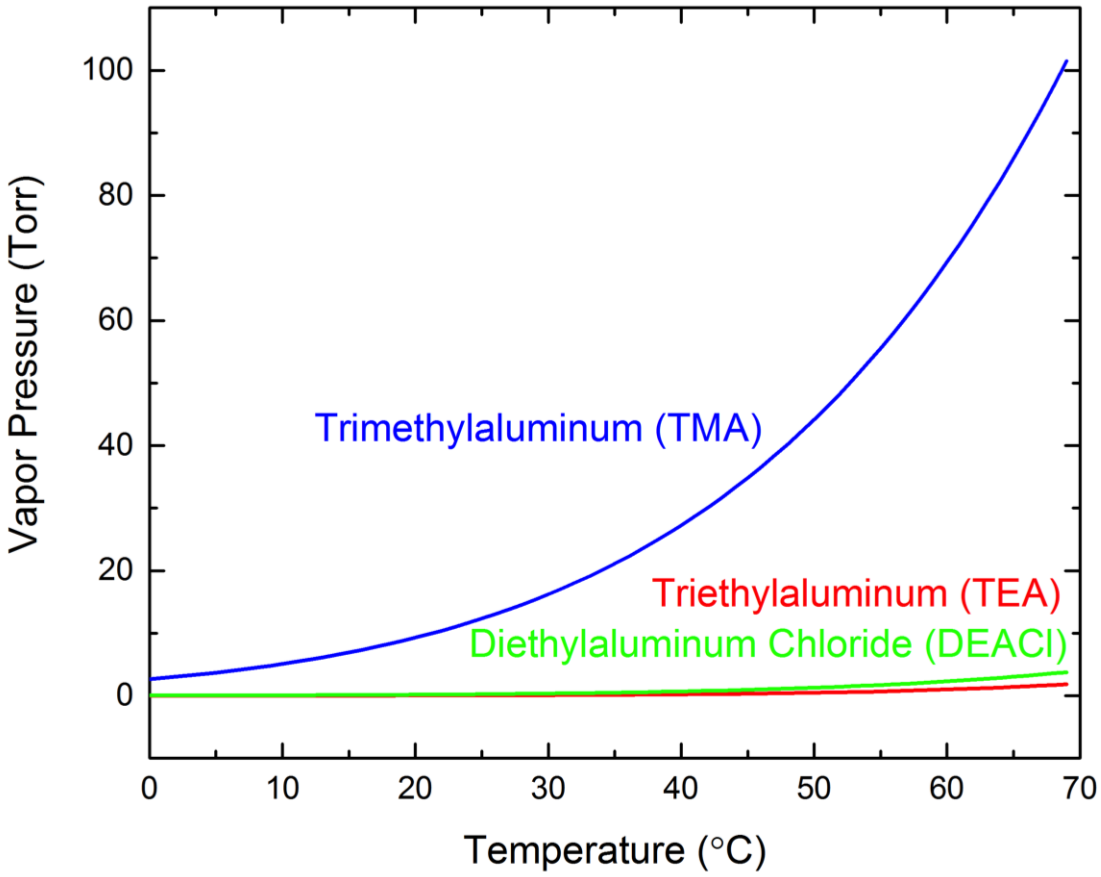

Figure 2.3: TMA exhibits the highest vapor pressure with respect to temperature.

to TMA. This criterion led to the selection of TMA as the precursor of choice for our process.

As can be seen from figure 2.3, TMA has a room-temperature vapor pressure around one order of magnitude higher than the other two other Al precursors shown.

2.4 Overview of trimethylaluminum

Trimethylaluminum (TMA) is a pyrophoric organometallic compound which is a liquid at room temperature with a corresponding vapor pressure of 11 Torr at 20 °C [10]. It has been used to synthesize aluminum thin films in a hydrogen plasma using a PECVD process [19–22]. As with other organometallic precursors, if the process is not carefully

controlled, TMA can dissociate in an undesirable fasion, resulting in carbon incorporation.

2.5 Fourier Transform Infrared Spectroscopy Characterization

Fourier Transform Infrared Spectroscopy (FITR) was used to characterize the surface chemistry of as-produced aluminum nanoparticles and monitor their oxidation over time. The characterization technique involves passing infrared radiation through a sample with a detector measuring the amount of light transmitted through the sample at varying frequencies. This information characterizes the sample, providing a molecular "fingerprint" of the bonds present and at which they resonate. Functional groups such as ketones, hydroxyls, hydrides and many others can be detected using FTIR.

Particulate films produced in the nonthermal plasma reactor were deposited onto pieces of polished sodium choride or bare silicon wafer.

2.6 X-Ray Diffraction Characterization

X-ray diffraction characterization was performed using a Bruker D8 Discover 2D X-ray diffractometer using a cobalt Kα source and a VÅNTEC-500 two-dimensional X-ray detector. JADE software by Materials Data Inc. (MDI) was used after data collection to convert all scans to a 1.54059 Å wavelength copper source as XRD data are typically presented in literature using copper sources.

Many nanoparticles samples produced in a TMA/Ar plasma reactor and deposited on substrates such as a piece of glass or silicon wafer were scanned under ambient conditions. Their exposure to air before scanning typically resulted in the formation of embers and oxidation of these nanoparticles. Eventually as-produced nanoparticles synthesized in the reactor were transferred via a load-lock system (or "pushrod") to a glovebox filled with nitrogen gas to atmospheric pressure.

Inside the glovebox, samples were transferred to a thin walled boron-rich capillary tube (Charles Supper Company Inc.) and stuffed with silicon vacuum grease. The capillary tubes had an outer diameter of 1.5 mm, a wall thickness of 0.01 mm and 80 mm

in length. The purpose of the vacuum grease was to temporarily prevent the nanoparticles from being exposed to air after removal from the glovebox. The capillary tube containing the sample was subsequently flame sealed to form an ampule. This allowing for long-term air-free storage and XRD characterization of nanoparticles synthesized in the reactor.

2.7 X-ray Photoelectron Spectroscopy Characterization

X-ray photoelectron spectroscopy is a surface measurement technique that can provide the elemental and chemical composition of a sample. It involves irradiating the surface of a sample with X-rays in a high-vacuum system. The energy from the X-ray can transfer this energy to an electron bound to an atom and ejecting. The freed electron's kinetic energy depends on its binding energy and the energy of the incident X-ray. The binding energy of an electron is the difference between the energy of its parent ionized atom vs the atom's neutral state. Every element has a characteristic set of binding energies linked to each of its atomic orbitals. Once the binding energies of a sample are obtained and displayed as peaks, they can be compared to known reference binding energies.

XPS characterization discussed in chapter 3 was performed using a Surface Science SSX-100 instrument using monochromated Al K X-rays and operating with an adjustable spot size of 50 μm through 800 μm. Its energy resolution is less than 0.8 eV with a binding energy measurement range of 0-1000 eV. This instrument was not capable of performing air-free analysis of samples.

XPS characterization discussed in chapter 4 was performed using a PHI Versa Probe III XPS instrument (ULVAC-PHI Inc.) with a monochromated Al K_α 1486.6 eV X-ray source. Unlike the XPS instrument previously described, the main advantage of using the PHI Versa Probe III was that it featured a load-lock compartment. This allowed for air-free transfer of as-produced nanoparticles into the instrument via a sample transfer connected to the main chamber. This made it possible to scan as-produced aluminum nanoparticles without exposing them to air. The system's base pressure was 5.0 x 10^{-8} Pa. During scanning, the pressure rose to about 1.0 x 10^{-6} Pa.

The nanoparticles were deposited on a 1 cm^2 piece of silicon wafer. The sample

was transferred to an air-free nitrogen atmosphere glovebox post-synthesis. The wafer was taped using conductive carbon tape to a stainless steel holder, which was subsequently sealed shut. The sample holder was attached to the transfer chamber of the XPS instrument, with the surrounding atmosphere pumped down, filled with nitrogen and then pumped down once more in order to load the sample into the high vacuum measurement chamber. The x-ray spot size 0.2 x 0.2 mm^2 with a power of 50 W under 15 kV.

Atomic percentages present in a sample were calculated from broad, survey scans using the Multipak software provided with the XPS instrument. For high resolution spectra, the lowest binding energy C (1s) peak was set to 285.0 eV and used as a reference for other binding energies found in the sample. All high resolution binding energy values were shifted by the the reference C (1s) peak. Curve fitting of peaks found in high resolution scans were comprised of a Gaussian/Lorenzian function, designed to minimize the chi-squared value of the fit. The Gaussian function contribution to all fited curves was no lower than 80%.

2.8 Transmision Electron Microscopy Characterization

Transmission electron microscopy (TEM) uses a beam of high energy electrons instead of light (as used in light microscopes) to image objects on the order a few angstroms in size. TEM imaging also allows one to view crystallographic planes or lattice fringes of crystalline nanoparticles. The spacing of the fringes corresponds to the that of a lattice plane. TEM was used to determine particle size, composition and crystallinity, if any.

Two transmission electron microscopes were used to characterize nanoparticles made in the nonthermal plasma reactor. The first was a Tecnai T12 microscope, which can perform imaging, diffraction and energy-dispersive X-ray spectroscopy (EDS). EDSs provides elemental composition of a sample by focusing a beam of electrons at a sample. If the beam collides with an electron in an outer shell of the atom and ejects it. Subsequently an electron from an even higher energy shell will drop down to replace it, giving off energy in the form of an X-ray. Since the energies measured are representative of a particular element, this allows for the identification of various elements present in a sample.

The second transmission electron microscope used was an FEI Titan G2 60-300 STEM operating at 300 keV, 25 mrad convergence angle, 150 pA beam current with imaging performed by Jacob Held of the Mkhoyan Group at the University of Minnesota. This instrument was used for imaging nanoparticles and performing electron energy loss spectroscopy (EELS). EELS measures the change in kinetic energy of electrons after interacting with a sample. It allows one to determine which type of atoms and chemical structure is present. This technique was used to determine whether the core of air-exposed nanoparticles produced in the Ar/H_2/TMA reactor contained elemental aluminum or an oxide.

2.9 Optical Emission Spectroscopy Characterization

Optical emission spectroscopy (OES) is a noninvasive plasma diagnostic method that is used to determine its composition. The energy provided to the plasma causes ionization of atoms. Freed electrons can undergo elastic collisions with atoms in the gas, exciting the atom's valence electrons to empty, higher energy orbitals. When those electrons relax energetically back to their valence orbitals, they give off energy in the form of a photon. The energy of these emitted photons are measured as different wavelengths of light. The emission of element in the periodic table is composed of characteristic wavelengths. The emission from a plasma during a chemical reaction can be compared to reference spectra of elements one expects to encounter. This in-situ measurement technique makes it possible to determine which species (e.g. radicals) are present during a chemical reaction proceeding within the plasma.

The quartz tube containing the discharge coated the inner walls over time as particles formed. As a result, the measured light intensity emitted from plasma through this coating would decrease over time. More precise optical emission measurements of the $TMA/Ar/H_2$ plasma would require sampling the light emission through a clean window not coated with thin films or nanoparticles. As a compromise, an Ocean Optics HR4000 spectrometer with nominal detection limits ranging from 200-1100 nm was used to gather optical emission data from the discharge thanks to its faster sampling time, but lacked finer resolution.

The HR4000 spectrometer by Ocean Optics was used to monitor the optical emission

from the plasma. Its real-time measurements collected from the plasma were displayed and recorded using software provided by Ocean Optics. Each measured spectrum consisted of 50 averaged scans. All scans included in the average had integration time of 20 msec.

OES characterization was used to study the formation of aluminum nanoparticles in an Ar/H_2/TMA plasma. The goal of this experiment was to identify any spectral trends in the plasma when parameters such as gas flow rates, pressure or power changed.

Chapter 3

Plasma synthesis without hydrogen gas

3.1 Nanoparticle synthesis without hydrogen gas

As a first approach, TMA was fed into in an argon-only plasma. These experiments were performed to determine whether it was possible to produce aluminum nanoparticles without the use of a reduction agent and evaluate the properties of these particles. These nanoparticles synthesized without hydrogen gas were noticeably pyrophoric and would form embers immediately upon air-exposure. Handling them required caution to avoid exposing these as-produced particles to air, which would oxidize them completely.

3.1.1 X-Ray Diffraction Characterization

Multiple attempts were made to synthesize aluminum nanoparticles in an Ar/TMA plasma. Nominal applied powers ranged from 5-80s W. System pressures ranged from 3.0-9.0 Torr with a carrier argon flow rate of 10 sccm. The flow rate of TMA was usually set to 1 sccm by the corresponding gas gas.

Initially the first set of samples made in the reactor were allowed to be exposed to air before scanning in XRD. Unfortunately they formed embers and turned from a brown to a white color, which indicated complete oxidation. Those air-exposed samples showed no crystallinity.

In order to protect the particles from air exposure, two types of air-free sample holders were used. The first holder consisted of a stainless steel bottom square piece with threaded holes on each corner and machined with a round cavity. As-produced nanoparticles were placed into this cavity in an inert glovebox. Thin mylar film was wrapped over the cavity on top of which a threaded metal piece placed. The air-tight seal was made by screwing the top piece into the bottom one. The second air-free sample holder that wound up being used more extensively was the boron-rich capillary tube discussed in section 2.6. An XRD data acquisition of air-free sample made in an Ar/TMA plasma at 20 W applied power with 1 sccm TMA and 10 sccm carrier Ar at a system pressure of about 9 Torr is shown in figure 3.1.

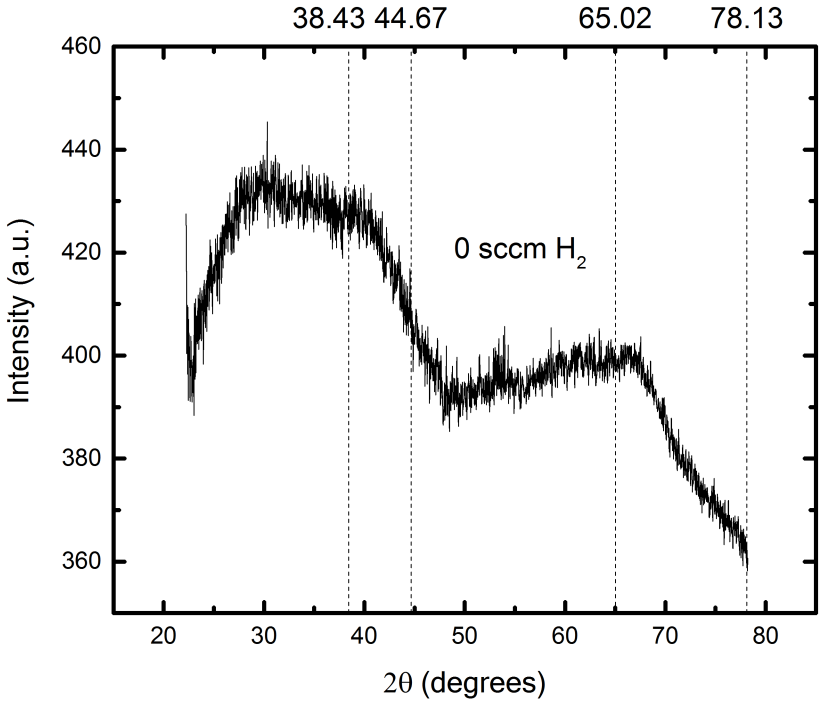

Figure 3.1: XRD acquisition of an air-free sample synthesized in an Ar/TMA plasma at an applied power of 20 W. The carrier Ar flow rate was 10 sccm. The TMA flow rate was 1 sccm at a system pressure of about 3 Torr. The nanoparticles were sealed in a metal holder with 50 μm tape sealed over the sample to prevent air-exposure. The acquired data showed no evidence of crystallinity.

The air-free sample showed no crystallinity using XRD characterization. This suggested that chemistry being used in the plasma to make the nanoparticles was not capable of producing elemental aluminum and would require a different approach.

3.1.2 X-ray Photoelectron Spectroscopy Characterization

As-produced nanoparticles were characterized using XPS to determine whether the aluminum residing in the sample was in elemental or oxide form. The nanoparticles were produced in a 20 W Ar/TMA plasma with flow rates of 1 sccm TMA and 10 sccm carrier Ar at a system pressure of about 9 Torr.

A Surface Science SSX-100 instrument was used to acquire data from the sample. Since it was not possible to insert a sample into the instrument without air exposure, the sample was introduced to ambient conditions before insertion into the Surface Science SSX-100. Unfortunately upon exposure to air, embers formed immediately on the sample, which likely oxidized it completely.

A high resolution scan of the sample in the region of Al (2p) saw one large peak whose best fit matched aluminum oxide reference at a binding energy of 72.25 eV. The high-resolution data are shown in figure 3.2.

As evident from the data, there was only one peak found in the Al (2p) region, which matched best with aluminum oxide reference. Judging from XPS alone, it is possible that the particles contained crystalline aluminum before air-exposure. On the other hand, the air-free XRD data acquisition of an air-free sample showed only an amorphous sample.

3.1.3 Transmission Electron Microscopy

Nanoparticles synthesized in the Ar/TMA plasma were produced using the same conditions as described in sections 3.1.1 and 3.1.2. The nanoparticles were deposited on holey carbon coated TEM grids sold by Structure Probe, Inc. An FEI Tecnai T12 transmission electron microscope was used to image the nanoparticles. Figures 3.3 and 3.4 show some representative nanoparticles with a 50 nm scale bar for size referencing.

The average diameter of the particles synthesized were about 30nm in diameter. Aluminum nanoparticles exposed to air will have an oxide shell that can range from 1-5

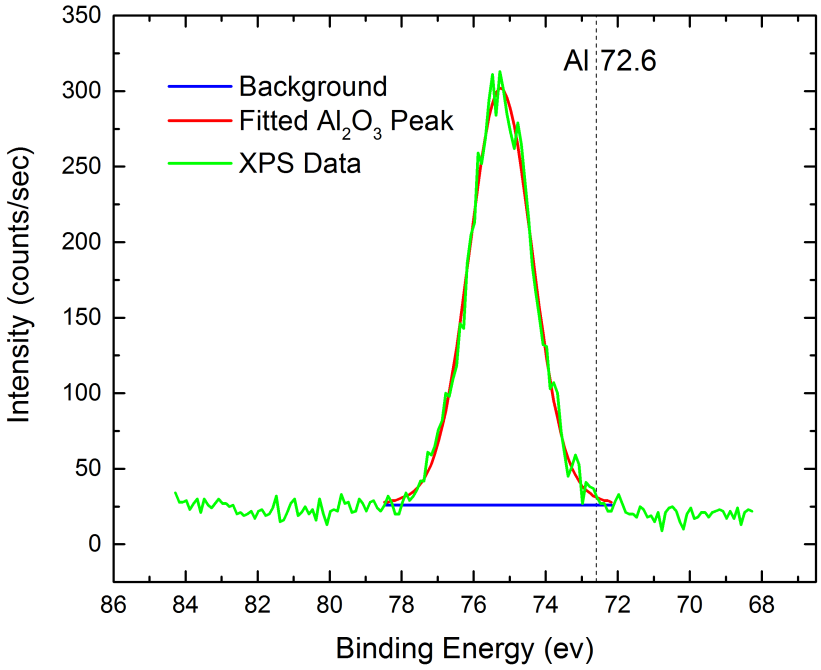

Figure 3.2: XPS high-resolution surface scan of an air exposed sample synthesized in an Ar/TMA plasma at an applied power of 20 W. The carrier Ar flow rate was 10 sccm. The TMA flow rate was 1 sccm at a system pressure of about 9 Torr. The fitted peak in the Al (2p) region best matched aluminum oxide reference.

nm. The nanoparticles shown here, do not show a contrast between the core and shell of the particle.

EDS measurements are shown in figure 3.5 with copper and carbon removed (since they were also present on the TEM grid before deposition). The EDS measurements showed the ratio of oxygen to aluminum was around 1.5, which corresponds closely to the 3/2 ratio of aluminum oxide (Al_2O_3).

Considering that the air-exposed nanoparticles possessed no noticeable oxide shell when observed using transmission electron microscopy, this indicates that the Ar/TMA plasma was not capable of producing crystalline elemental aluminum nanoparticles. Therefore the chemistry of the plasma process had to be rethought.

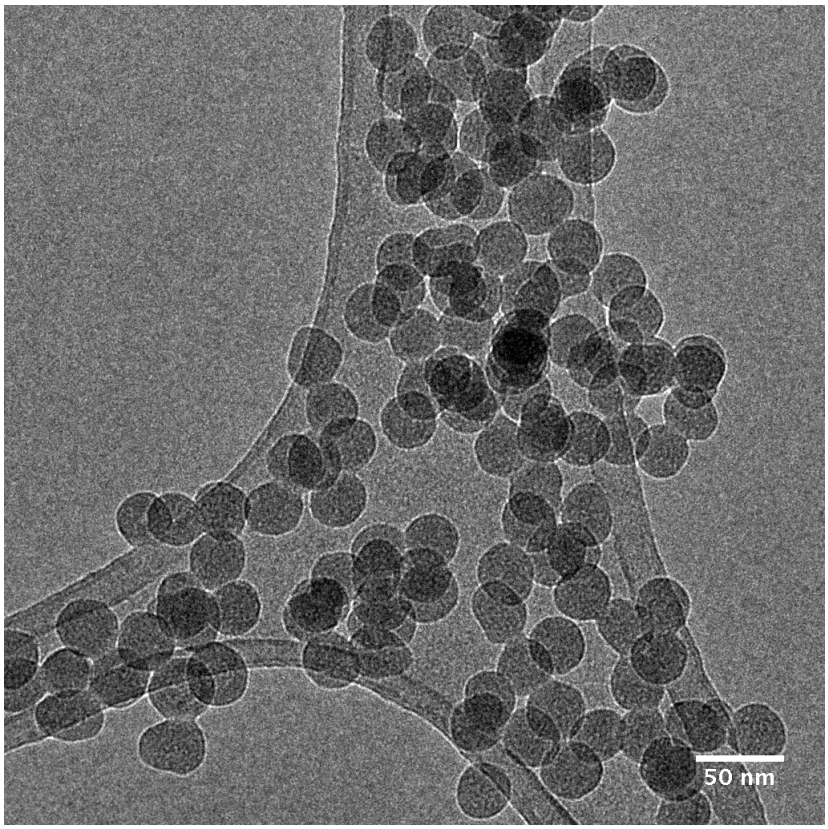

Figure 3.3: TEM image of nanoparticles synthesized in an Ar/TMA plasma at 20W using 1 sccm TMA and 10 sccm carrier Ar. The nanoparticles were exposed to air in order to insert them into the instrument. The diamter of the particles ranged from around 25-30 nm.

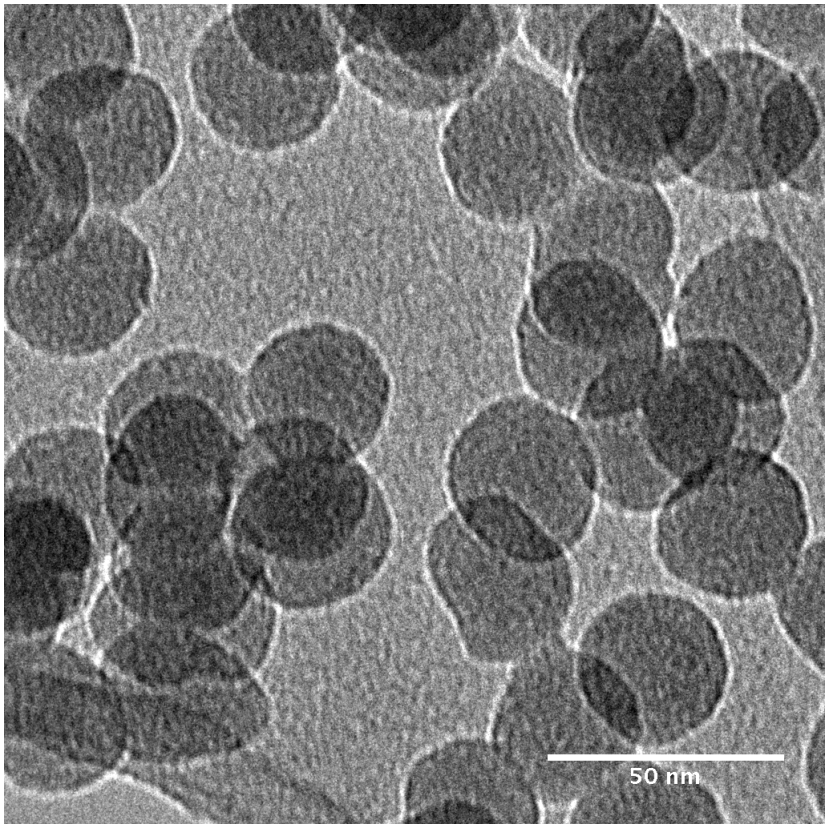

Figure 3.4: A closer view of the nanoparticles synthesized in an Ar/TMA plasma at 20W using 1 sccm TMA and 10 sccm carrier Ar. The nanoparticles were exposed to air in order to insert them into the instrument. A closer inspection of these nanoparticles revealed no discernible oxide shell

.

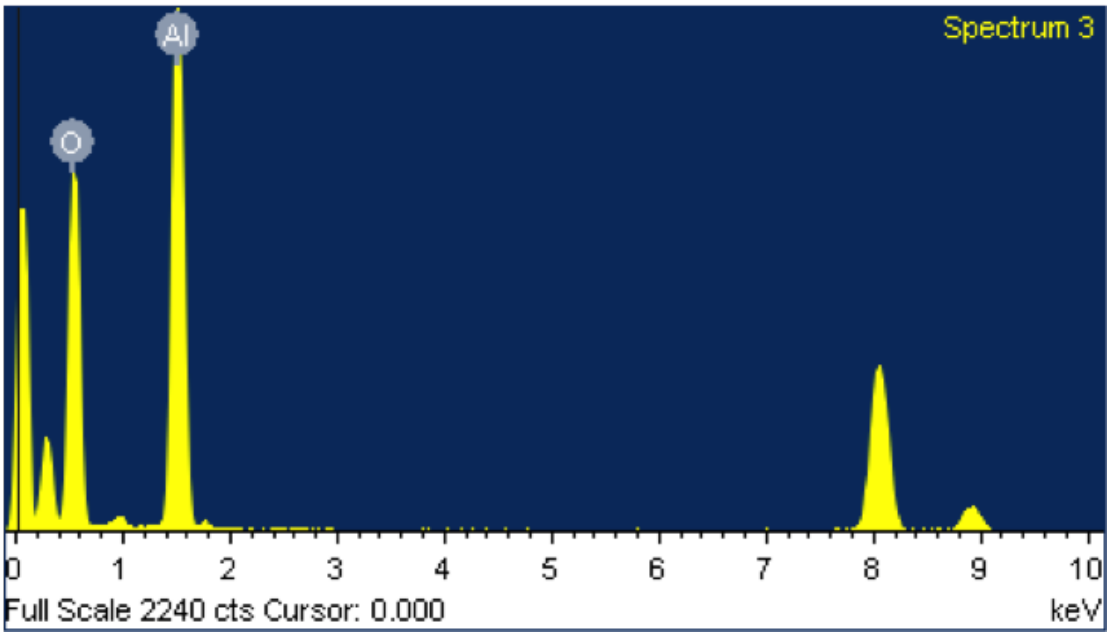

Figure 3.5: EDS data acquisition nanoparticles synthesized in an Ar/TMA plasma at 20W using 1 sccm TMA and 10 sccm carrier Ar. The nanoparticles were exposed to air in order to insert them into the instrument. The ratio of O/Al was nearly 1.5

.

Chapter 4

Nanoparticle Synthesis With Hydrogen Gas

4.1 Using Hydrogen As A Reducing Agent

Masu *et. al* were able to successfully deposit pure aluminum films using a 90W TMA/H_2 RF plasma [19]. Therefore a hydrogen gas line was connected to our reactor. Rather than simply using an Ar/TMA plasma, an Ar/H_2/TMA plasma was used instead. Adding hydrogen gas made it possible to convert the CH_3 methyl groups of TMA into alkanes such as methane (CH_4) or ethane (C_2H_6) with the extra H atoms provided. They were able to form aluminum films only when TMA undergoes what they termed "weak-excitation". Weak-excitation meant decomposing TMA within the plasma into chemical species such as $Al(CH_3)_2$ or $Al(CH_3)$. Once those species reached the substrate, they would react with hydrogen gas to evolve methane, leaving behind only solid thin films of aluminum.

Without the addition of hydrogen gas, TMA's leaving alkyl groups would need to abstract hydrogen from other TMA molecules as discussed by Masu *et. al* [19]. The previous Ar/TMA plasma was not able to synthesize aluminum because it likely lacked a sufficient amount of hydrogen necessary to reduce aluminum atoms in TMA to their elemental form.

Mass spectroscopy analysis performed by Masu *et. al* showed that the plasma was capable of decomposing TMA dimer molecules in the presence of hydrogen to form

ethane [19]. Each of the two CH_3 groups (or bridging groups) bonded to both aluminum atoms in TMA joined together to form C_2H_6. The remaining parts of the TMA dimer such as $Al(CH_3)_2$ and $Al(CH_3)$ would then react at the substrate surface in the presence of hydrogen to evolve methane gas.

The formation of stable gas species such as CH_4 and C_2H_6 in the plasma made it possible to form pure aluminum films without carbon contamination. To demonstrate the importance of adding hydrogen to the plasma, Masu *et. al* also attempted to synthesize Al films using a 90W H_2 microwave (μ-wave) plasma, a 36W Ar RF plasma and a 23W Ar μ-wave plasma. Optical emission spectroscopy was used to observed all of these plasmas. All except RF/H_2 showed atomic aluminum emissions between 200-400nm. This confirmed that only the RF/H_2 plasma was capable of achieving the weak-excitation of TMA, rather than fully decomposing TMA into Al atoms in the gas-phase. Plasma diagnostic measurements showed that electron density (number of electrons per unit volume), not electron temperature was the most crucial parameter for controlling the decomposition of TMA in a hydrogen plasma to form Al films at the substrate [20].

Two issues were likely plaguing our synthesis of aluminum nanoparticles using an Ar/TMA glow discharge. First we did not have enough hydrogen atoms to react with the leaving methyl radicals to form stable leaving groups such as methane. Secondly our electron density was likely too high. Plasma density measurements by Masu *et. al* with respect to input power showed their RF Ar/TMA discharges possessed electron densities nearly an order of magnitude higher than the corresponding RF H_2/TMA plasma. This result may be surprising considering the ionization energy of a single hydrogen atom is 13.61 eV whereas argon's ionization energy is 15.76 eV [23]. The ionization energy alone, however, does not determine the electron density in a plasma. Alternative electron energy loss mechanisms besides ionization must be accounted for in a plasma as well.

In monatomic plasmas such as argon, there are three ways for electrons to lose energy: elastic collisions with argon atoms (total kinetic energy and momentum is conserved during the collision), excitation collisions that promote an electron to a higher energy state and finally the ionization of the atom's electron.

Hydrogen gas, on the other hand, is diatomic with a chemical bond linking two

hydrogen atoms together with each atom sharing a full duet. For a monatomic gas such as argon, its atoms can only acquire translational kinetic energy. For molecular gases such as hydrogen, their chemical bond provides the molecule three extra degrees of freedom. They can acquire vibrational energy when the bond is stretched or compressed and rotational energy when the molecule's angular velocity about the center of the bond changes. Consequently, since there are more ways to energetically excite hydrogen molecules in a plasma, a smaller percentage of applied power is converted into the ionization of hydrogen. Since Argon is a noble gas, it does not need to bond with itself to achieve a full octet, which means more applied energy is consumed forming Ar^+ ions.

4.2 Obtaining An Initial Recipe To Produce Elemental Aluminum Nanoparticles

Based on the work on the successful PECVD [19–22] and atomic layer deposition (ALD) of aluminum films using RF hydrogen plasmas, hydrogen gas was added to the TMA/Ar plasma. The purpose of H_2 was to reduce the Al-C organometallic bonds in TMA and evolve stable gaseous hydrocarbon leaving groups, leaving only aluminum atoms behind. At room temperature, the formation of solid aluminum would be thermodynamically more stable and thus promote the formation of aluminum nanoparticles through homogeneous nucleation in the gas-phase.

Another study by Masu *et. al* [21] noticed that aluminum thin-film deposition rates increased with plasma power density (W/cm^3) without carbon incorporation in a TMA/H_2 RF plasma. On the other hand, if the power density was increased too far, carbon contamination was observed due to excessive decomposition of TMA. Too little applied power resulted in no Al deposition. The synthesis of Al nanoparticles in a TMA/Ar/H_2 plasma may also allow for only a fixed power range in order to avoid carbon contamination.

Precursor flow rates are kept low in metal CVD processes to suppress nanoparticle formation. This reduces the concentration of metal atoms per unit volume in order to prevent gas-phase homogeneous nucleation. Masu *et. al* [19] used approximately a 300/1 ratio of H_2/TMA (assuming a standard temperature and pressure of 273.15 K & 1 atm, respectively.)

To encourage particle formation, an appropriate reducing agent to precursor ratio had to be determined for our system. Since aluminum thin-films exhibit mirror reflection, preliminary reactions focused on the depositing of gray, reflective films, instead of the thick dark brown coatings seen between the electrodes where the TMA/Ar plasma was located

Preliminary experiments focused on depositing gray, reflective coatings between the electrodes. Initially a 490/1 ratio of hydrogen gas to TMA vapor (50 sccm H_2/ 0.02 sccm TMA) was used to ensure the formation of thin films. In addition a high ratio of H_2/TMA would also ensure appropriate stoichiometry necessary for reducing TMA to Al. The reflective film formed predominately between the electrodes inside the glass tube. To examine the crystallinity of the reflective films, silicon wafers were taped on the inner diameter of the glass tube between the electrodes. XRD characterization of the reflective thin films did not show crystallinity regardless of how much nominal applied power was used (10-30W).

To promote particle formation and investigate the crystallinity of nanoparticles synthesized in the TMA/Ar/H_2 plasma, the flow rate of hydrogen gas was decreased to 50 sccm, with TMA's flow rate increased to 1 sccm. Increasing the concentration of TMA in the plasma would allow for a higher concentration of aluminum atoms to exist in the plasma, encouraging homogeneous nucleation and thus nanoparticle formation.

Nanoparticles containing crystalline elemental aluminum were produced at nominal powers of 10 W and 15 W. XRD scans of the 10 W and 15 W samples are shown in figure 4.1. The dotted lines denote reference face centered cubic (FCC) aluminum.

We can see from these scans that crystalline aluminum was successfully synthesized using a Ar/H_2/TMA plasma. Without the use of an ampule to protect these nanoparticles from air-exposure, they would have oxidized completely and lost their crystallinity.

4.2.1 XPS Characterization

XPS was used to determine which elements were present on the surface and inner core of air-free as-produced nanoparticles synthesized using the original recipe. It was also used to determine what percentage of the nanoparticles produced in the reactor were composed of elemental aluminum, aluminum oxide or carbon byproducts.

The as-produced particles were not sufficiently conductive and charge neutralization

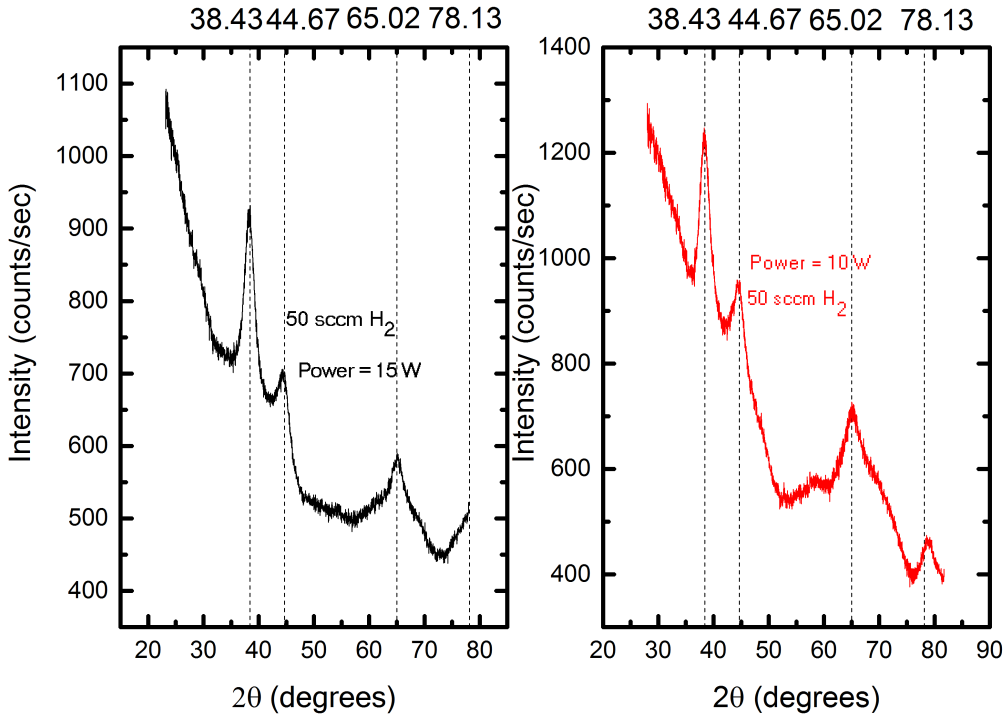

Figure 4.1: XRD acquisition of aluminum nanoparticles sealed in an ampule synthesized at 10 W of nominal applied power using 50 sccm H_2, 10 sccm carrier Ar and 1 sccm TMA. This demonstrates that the Ar/H_2/TMA nonthermal plasma is capable of producing aluminum nanocrystals. Dotted lines denote standard FCC elemental aluminum diffraction peaks.

was used before performing high resolution scans. In order to probe deeper into the core of the particle an Ar^+ etching system was employed to perform depth profiling with a material removal rate of 3.0 nm/min. A combination of survey and a subsequent high resolution scan was performed on the surface of the nanoparticles, 1.5 nm (30-sec etch) under the surface and 3.0 nm (60-sec etch) under the surface. These high resolution spectra were collected using a 0.05 eV step size and 26 eV pass energy for the Al(2p), C(1s) and O(1s) peak regions.

Survey scans of the outer layer, 1.5 nm and 3.0 nm into the nanoparticles showed that aluminum, oxygen and carbon were present. A summary of the survey measurements displayed with atomic percentages with corresponding to each scan are shown in figure

4.2.

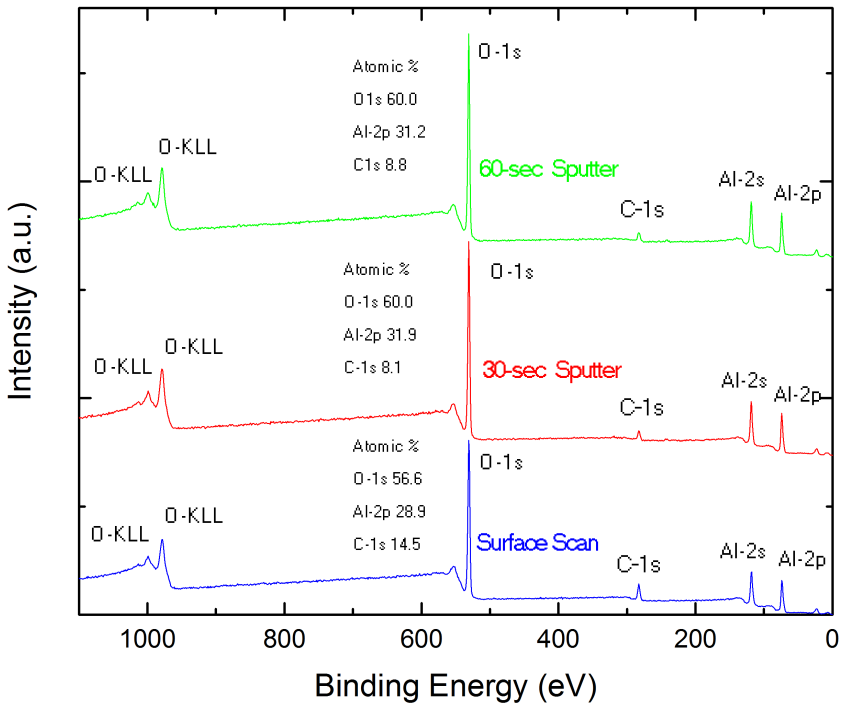

Figure 4.2: XPS depth-profiling of aluminum nanoparticles synthesized in a 15 W $Ar/H_2/TMA$ discharge with 1 sccm TMA, 10 sccm carrier Ar and 50 sccm H_2. Carbon percentage decreased by 44% after 1st etch to the surface. The 2/1 ratio of O/Al changed little with depth profile.

As shown by the survey scans, carbon was present in the sample. There are two possibilities to explain the presence of carbon on the surface. It may have been a result of user contamination while the sample was being transferred from the load-lock to the XPS air-free sample holder inside the glovebox. Another possibility is that not all methyl groups bonded to aluminum in TMA were completely removed while undergoing reactions inside the $TMA/Ar/H_2$ plasma. The later would explain why the atomic percentage of carbon did not reduce to zero after etching.

The results of a high resolution scan in the Al (2p) region after 1.5 nm (30 sec) of

etching with curve fits are shown in figure 4.3. It reveals that three types of aluminum were present.

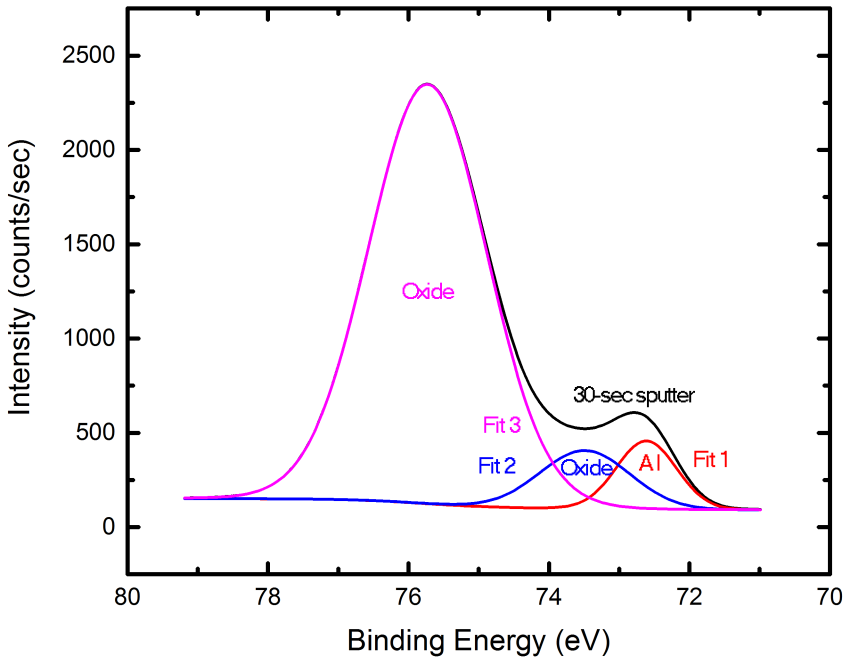

Figure 4.3: XPS high-resolution scan of aluminum nanoparticles at a depth of 1.5 nm from the surface. The sample was synthesized in a 15 W Ar/H_2/TMA discharge with 1 sccm TMA, 10 sccm carrier Ar and 50 sccm H_2. A majority of the the aluminum atoms measured came from aluminum oxide or another oxidized form such as an aluminum hydroxide.

The smallest fitted peak occurring at an energy of 72.61 eV matches elemental aluminum. It only contributed to 7.01% of the overall area occupied by the fitted curves, indicating only a small fraction of aluminum in the sample did not oxidize. The largest observed peak observed at a binding energy of 75.73 eV closely matches alumina (Al_2O_3) and occupied 84.06% of the total area occupied by the fitted curves. The third peak observed in the region of aluminum's binding energy was observed at a binding energy of 73.49 eV and occupied 8.93% of the overall area occupied by the fitted curves. This peak potentially matches with a form of aluminum hydroxide.

XPS characterization demonstrated that the elemental composition of the nanoparticles produced using the original recipe was mostly uniform, except for the extra amount of carbon on the sample's surface.

4.2.2 FTIR Characterization

FTIR was used to elucidate which types of chemical species were present on the surface of aluminum where XPS analysis fell short and could not provide a complete picture. Particulate films were deposited on two pieces of polished sodium choride. The first film was produced using the same flow rates as the original recipe (50 sccm H_2, 10 sccm carrier Ar and 1 sccm TMA). The second film was synthesized using only 25 sccm H_2, while holding other flow rates fixed.

The as-produced films were immediately transferred to the nitrogen filled glovebox and characterized in FTIR using a Bruker Alpha IR spectrometer with a transmission module. The absorbance of each fresh film was measured after synthesis and 15 hours later after remaining in the glovebox overnight. The absorbance of both samples as-produced and after 15 hours in the glovebox are shown in figure 4.4.

The FTIR measurements of nanoparticles made in the $Ar/H_2/TMA$ plasma also possess some of the same features as an aluminum oxide film deposited using TMA vapor, N_2O and Helium (He) gases in another PECVD reactor by Kim *et. al* [24].

Scans of both the 25 and 50 sccm H_2 samples confirm that aluminum-oxygen (Al-O) bonds are present on the surface of the nanoparticles. There is also evidence an Al-CH_3 peak centered around 1200 cm^{-1}, an aluminum-hydride (Al-H) peak centered around 1725 cm^{-1}, an alkyl C-H peak (likely from the same CH_3 group bonded to aluminum) between 2800-3000 cm^{-1} and finally an O-H stretching mode in the 3000-3500 cm^{-1} range [24].

A zoomed-in view of the four functional group peaks is shown in figure 4.5.

4.2.3 STEM Characterization

Aluminum nanoarticles synthesized using the original recipe and coated with approximately 10 nm of amorphous silicon in a separate reactor to encapsulate the particles and protect them from air-exposure. Since the primary particle size was only 8-10 nm in

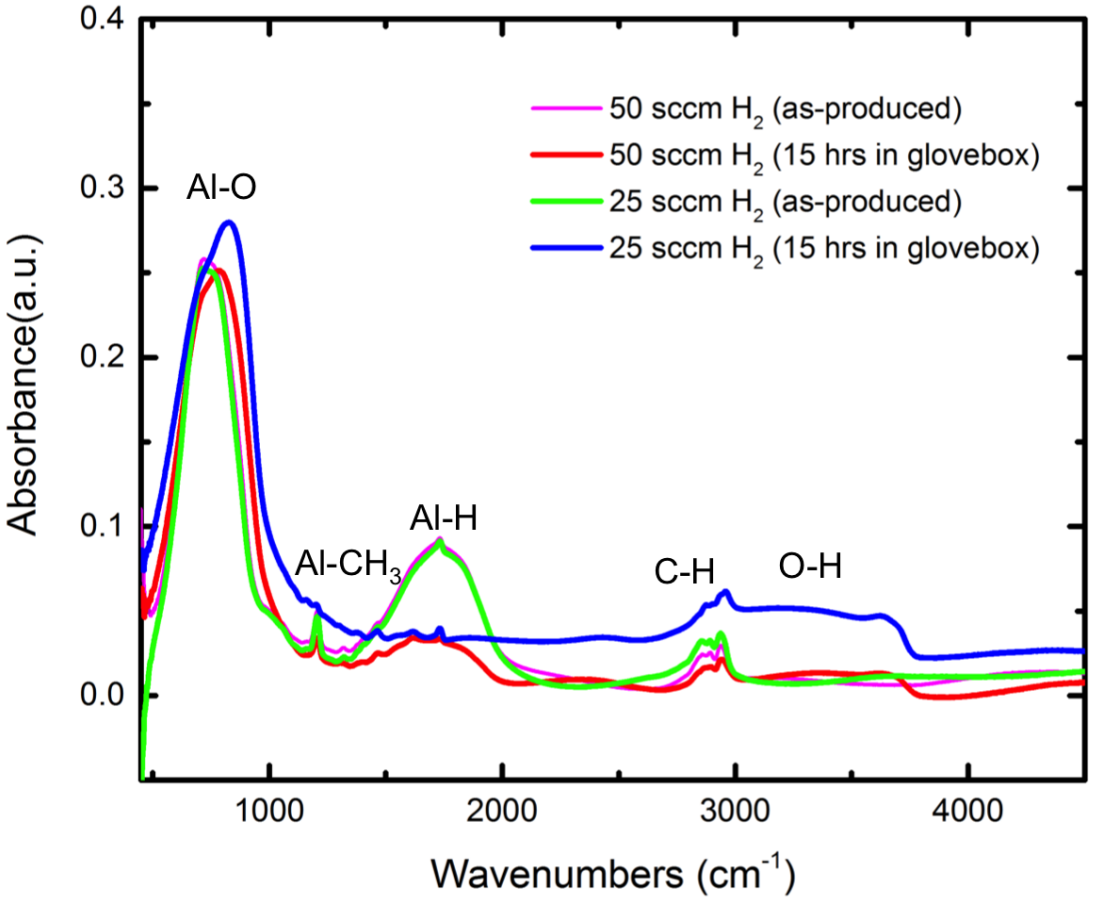

Figure 4.4: Survey FTIR transmission scans of samples synthesized using 1 sccm TMA, 10 sccm carrier Ar and 25 or 50 sccm H_2 plotted as sample absorbance vs wavenumber. Both samples show definite a Al-O bond as well as Al-C and Al-H bonds

diameter, air-exposure could lead to an alumina coating up to 5 nm thick, oxidizing the entire particle. The aluminum particles were deposited on copper coated TEM grids, precleaned using an O_2 plasma to remove excess carbon contamination. The sample was imaged using a Scanning transmission electron microscope (STEM) to determine particle size and chemical composition. Images of the particles with the film coating are shown in figure 4.6.

Particle imaging revealed that many of the nanoparticles produced in the reactor had agglomerated mid-flight before depositing on the TEM grid. This may have occurred

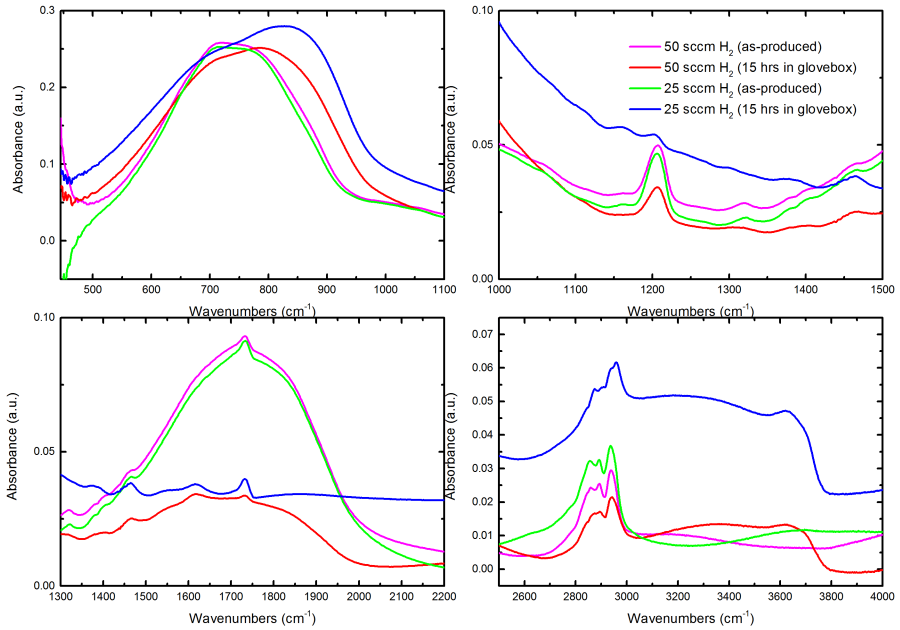

Figure 4.5: Zoom of FTIR transmission scans of samples synthesized using 1 sccm TMA, 10 sccm carrier Ar and 25 or 50 sccm H_2 in an $Ar/H_2/TMA$ plasma and plotted as sample absorbance vs wavenumber. Both Al-CH_3 and Al-H peaks disappeared 15 hours after exposure to the glovebox atmosphere.

while the particles were leaving the plasma region, entering the downstream stainless-steel conical reducer before acceleration through the orifice and deposition onto the TEM grid. Previous STEM imaging of the as-produced Al nanoparticles indicated their size ranged from 8-10nm after air-exposure.

EDS mapping was used to determine the distribution of elements within the coated nanoparticles. The mapping is shown in figure 4.7.

Unfortunately, as figure 4.7 indicates, it appears that the amorphous silicon coating was unable to completely encapsulate the particle to prevent oxidation. In addition the sample's EELS spectrum matched more closely to Al_2O_3 reference than that of elemental aluminum.

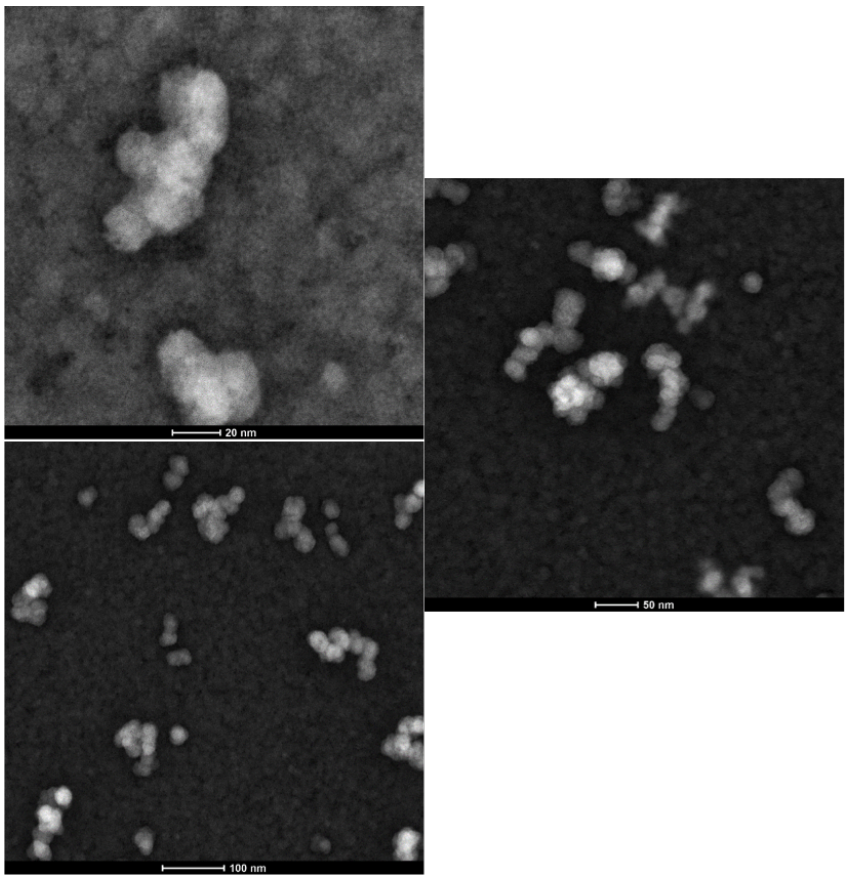

Figure 4.6: STEM images of aluminum nanoparticles synthesized using 50 sccm H_2, 10 sccm carrier Ar and 1 sccm TMA formed in an Ar/H_2/TMA discharge and covered with approximately 10 nm of an amorphous silicon film. The images indicate in-flight agglomeration occurred before deposition.

4.3 Flow Rate Studies

4.3.1 Hydrogen flow study

The initial recipe used to successfully synthesize nanocrystalline aluminum in the non-thermal plasma reactor used a flow rate of 50 sccm of H_2 along with 1 sccm TMA. As noted previously in chapter 3, the Ar/TMA plasma was unable to produce elemental aluminum detectable using XRD characterization. Therefore a minimum amount of hydrogen gas is required for reducing TMA into elemental aluminum. To determine the minimum amount of H_2 required, a flow rate study using an increasing amount of

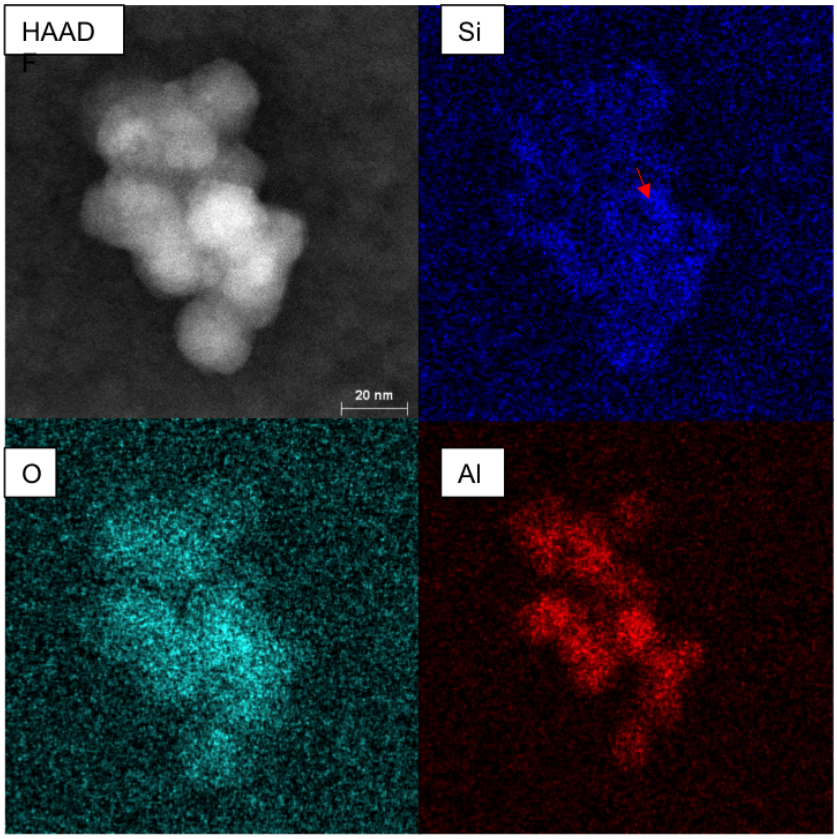

Figure 4.7: STEM EDS mapping of aluminum nanoparticles synthesized using 50 sccm H_2, 10 sccm carrier Ar and 1 sccm TMA formed in an $Ar/H_2/TMA$ discharge and covered with approximately 10 nm of an amorphous silicon film. Si appears to cover Al, but its decrease denoted by the red arrow combined with no corresponding reduction of O_2 indicates the particle had mostly oxidized.

hydrogen was conducted.

Table 4.1 shows the amounts of hydrogen and dilution argon gases used for a total combined flow rate of 100 sccm across all trials as well as the system pressures (averaged at the beginning and end of each run). The bubbler's pressure was held fixed around 100 Torr using the needle valve in order maintain a constant TMA flow rate of 1 sccm. The particles were accelerated through a rectangular slit orifice downstream of the plasma and impacted on a microscope glass slide. The electrode spacing was fixed at a distance of about 2.0 cm. The carrier argon flow rate was held fixed at 10 sccm for all trials. In addition the applied plasma power was held fixed at 15 W.

Table 4.1: **Hydrogen study conditions**

H_2 (sccm)	**Dilution Ar (sccm)**	**Average System Pressure (Torr)**
40	49	1.610
60	29	1.497
70	19	1.299
80	10	1.223
89	0	1.097

Deposition time was inversely proportional to the amount of hydrogen gas flowing. When the percentage of H_2 with respect to the total flow rate decreases, more particles were produced each minute. This suggests that the TMA vapor decomposed in a less controlled manner within the plasma. This type of behavior was also observed during the attempted synthesis of aluminum nanoparticles in an TMA/Ar plasma without the use of hydrogen as a reducing agent. The reaction time for each run continued to proceed until a sufficient amount of particles were deposited for XRD analysis by visually monitoring the process through vacuum view ports.

To prevent air exposure after deposition, the substrate was pulled inside the air-free load lock chamber connected to the reactor, filled with argon gas to atmospheric pressure and transferred to a nitrogen atmosphere glovebox. The load-lock chamber was opened inside the glovebox and the particles synthesized from each trial were transferred to their own respective thin-walled X-ray diffraction capillary tubes. The tubes were stuffed at the open end with silicon vacuum grease inside the inert glovebox environment and transferred outside to the ambient. The tubes were flame sealed to form thin ampules for XRD characterization. All six samples produced were scanned for a total of 30 minutes.

Each sample was scanned in the Bruker D8 Discover X-Ray Diffractometer for 30 minutes. Their measurement scans are shown in figure 4.8. The dotted lines denoted reference face centered cubic (FCC) aluminum.

Figure 4.8 confirms that a minimum amount of hydrogen gas was required to reduce TMA and form crystalline aluminum particles. There are two possible reasons for why a minimum of 70 sccm H_2 was required. First, the ratio of H_2/TMA may have been too low and more hydrogen reducing agent was required to form elemental aluminum.

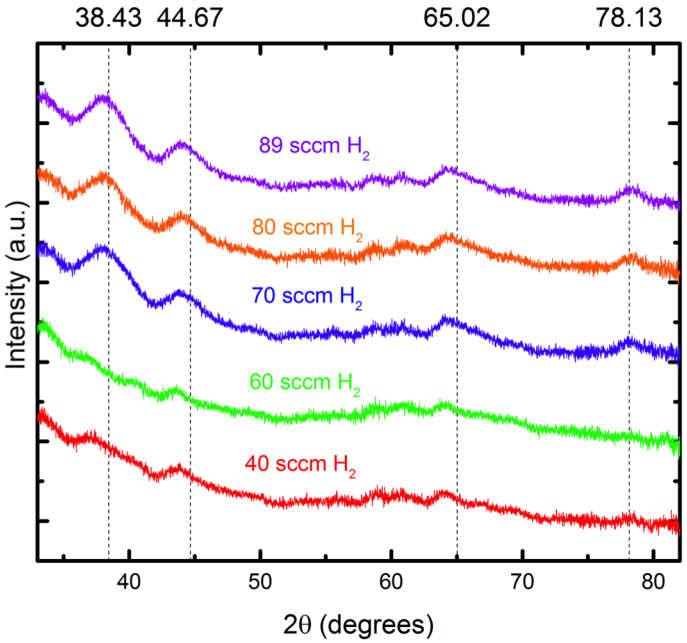

Figure 4.8: 30-min XRD data acquisitions of aluminum nanoparticles synthesized using 40-89 sccm H_2 in 15 W plasmas. The total flow rate used to produce each sample was 100 sccm. The TMA and carrier Ar flow rates were held constant at 1 sccm and 10 sccm, respectively. The dilution argon flow rate was set to maintain a total flow rate of 100 sccm. 70 sccm H_2 was the minimum amount required to produce nanocrystalline aluminim for 1 sccm TMA (dotted lines denote standard FCC elemental aluminum diffraction peaks).

On the other hand, the plasma conditions need to be considered as well. As noted in section 4.1 Masu *et. al* found that the "weak-excitation" of aluminum required low electron density [19]. When the percentage of hydrogen gas compared to the total flow rate was less than 70%, nanoparticles containing crystalline aluminum were not synthesized. Therefore it is possible that the percentage of monatomic argon gas was so high that it contributed to an exceedingly high electron density within the plasma. This high electron number concentration could have dissociated TMA into undesirable nanoparticulate aluminum byproducts, hindering the formation of elemental aluminum.

The crystalline 70-89 sccm H_2 nanoparticles were each scanned a second time for a longer duration of 3 hours to determine whether additional hydrogen flow produced sharper crystalline peaks. Their data are shown in figure 4.9 with dotted lines denoting

reference face centered cubic (FCC) aluminum peaks as in figure 4.8.

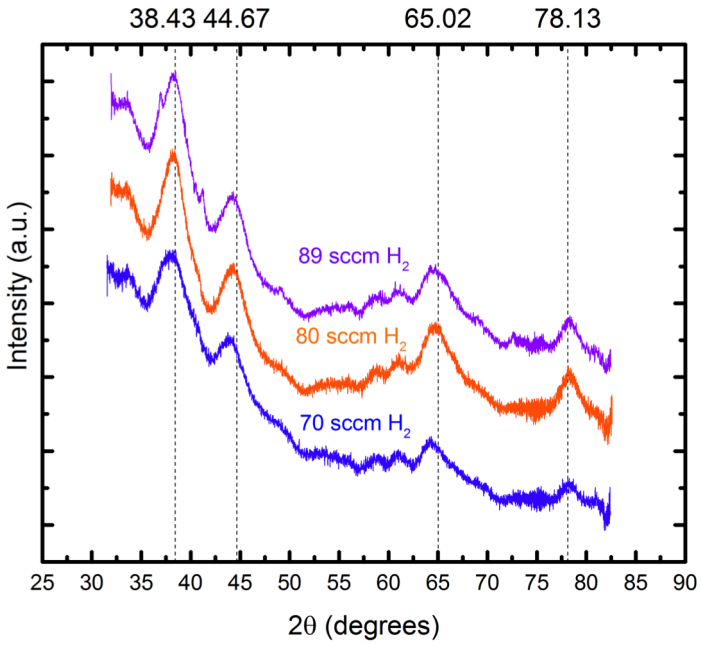

Figure 4.9: 3-hour XRD data acquisitions of aluminum nanoparticles synthesized using 70-89 sccm H_2 in 15 W plasmas. The total flow rate used to produce each sample was 100 sccm. The TMA and carrier Ar flow rates were held constant at 1 sccm and 10 sccm, respectively. The dilution argon flow rate was set to maintain a total flow rate of 100 sccm. The 70-89 sccm H_2 samples did not qualitatively exhibit a significant change in crystallinity vs flowrate. Dotted lines denote standard FCC elemental aluminum diffraction peaks.

Qualitatively the peaks from the 70-89 sccm H_2 samples looked similar. Nanocrystallite size was estimated using a 7th order pseudo Voigt background fit for consistency. The reported crystallite sizes of the three largest peaks were averaged to obtain a crystallite size. The reported crystallite sizes obtained from each crystalline sample were compared in table 4.2.

OES Characterization

To study the optical emission of the reaction plasma a 50 μm optical fiber was placed outside the glass tube between the electrodes (1.9 cm electrode-spacing) where the plasma was brightest. The conditions displayed in table 4.1 were repeated in order to

Table 4.2: **Hydrogen study crystallite sizes**

H_2 (sccm)	**Average crystallite size (Å)**
40	N/A
60	N/A
70	44
80	44
89	33

measure their respective optical emission spectra. Since the reaction conditions with the lesser flow percentages of hydrogen deposited a coating on the inner surface of the glass tube more rapidly, the emission of the 89 sccm H_2 plasma was recorded first. Conditions with decreasing percentages of hydrogen gas were subsequently scanned. Before turning the plasma on, a background measurement of the diffuse light from ceiling lamps and other light sources in the room was recorded. These background peaks were later subtracted from all emission spectra collected with the room's background light on.

Since the HR4000 spectrometer had not been recently calibrated, a light intensity correction factor was applied to all measured spectra. The correction factor was acquired by placing an optical fiber connected to the HR4000 spectrometer directly opposite an HL-3plus lamp (Ocean Optics) with a known spectral output inside a darkroom with the ceiling lamps shut off. The light emitted from the lamp was measured by the spectrometer and recorded. One disadvantage with this approach was that background light could be completely eliminated (e.g. brightness from the computer monitor recording the data). The spectrometer's measured intensities with respect to wavelength were compared with the expected lamp output. This comparison provided a scaling factor with respect to wavelength. If the HR4000 spectrometer measured more light than expected, its counts were scaled down. Otherwise its counts were scaled up if it measured less than expected from the HL-3plus lamp.

The plasma emission from each set of conditions was processed off-line by multiplying the difference between it and the room's background light with the post-correction obtained from the calibration lamp. All peaks contained in each spectrum were normalized by the height of their respective Ar peak occurring at 751.34 nm. Therefore

direct comparisons of absolute intensities between flow conditions is not possible. On the other hand, it is possible to compare the relative intensities of peaks within their respective spectrum.

The data are shown in figure 4.10.

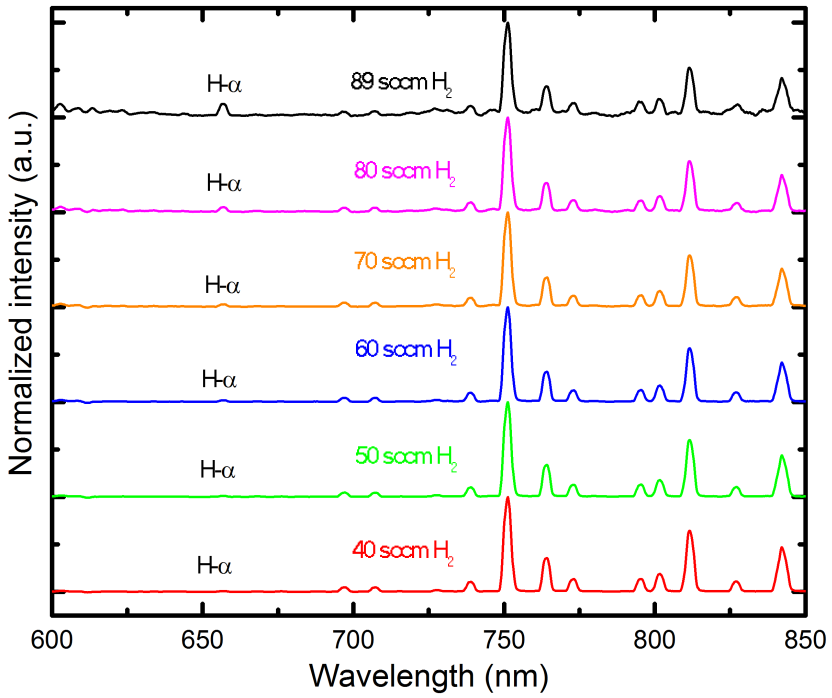

Figure 4.10: Optical emission spectroscopy was used to look for spectral trends in $Ar/H_2/TMA$ plasma consisting of varying amounts of hydrogen gas from 40-89 sccm. The 89 sccm H_2 condition exhibited the largest H-α peak relative to the Ar I peak at about 751 nm).

A comparison of the emission spectra for all conditions showed that the relative intensity of the H-α (indicative of atomic hydrogen) rose as the percentage of hydrogen gas flow increased. Therefore it appears that a minimum amount of atomic hydrogen was required in order to form crystalline elemental aluminum. This was achieved by flowing a higher percentage of hydrogen gas.

Masu *et. al* [19] also observed emission from H-α peaks in their PECVD of aluminum films when characterizing their 90 W RF H_2 discharge. This further demonstrates the importance of observing this spectral peak in the synthesis of elemental aluminum from TMA.

4.3.2 TMA flow study

To investigate what impact the H_2/TMA ratio had on the Al nanoparticle synthesis process, a second flow study was conducted. Table 4.3 documents the average reactor pressure (averaged at beginning and end of reactions), amount of carrier Ar, dilution Ar and TMA vapor used. The total flow rate was again fixed at approximately 100 sccm (neglecting the amount of TMA, which accounted for ≈1-2% of the total amount of gases in the reactor). The total amount of hydrogen gas flowing held constant at 80 sccm. The applied plasma power was held to 15 W across all trials.

Table 4.3: **H_2/TMA study conditions**

Carrier Ar (sccm)	**TMA (sccm)**	**Dilution Ar (sccm)**	**Average System Pressure (Torr)**
8	0.89	12	1.610
10	1.11	10	1.497
15	1.67	5	1.299
20	2.22	0	1.223

Reactions were allowed to proceed until a sufficient amount of particles were deposited on the glass substrate for XRD analysis. As the amount of TMA increased (with H_2 flow fixed), the deposition rate of nanoparticles increased. This again suggested that undesirable decomposition of TMA was occurring, resulting in the deposition of non-crystalline Al-containing nanoparticles.

Each sample was scanned in the Bruker D8 Discover X-Ray Diffractometer for 30 minutes. Their measurement scans are shown in figure 4.11. The dotted lines denote reference face centered cubic (FCC) aluminum.

The results of this flow study qualitatively showed as the H_2/TMA decreased, the crystalline peaks of the samples became broader with loss of peak intensity as well. This experiment demonstrated the importance of the H_2/TMA ratio. Without a sufficient amount of hydrogen gas flowing into the plasma region with respect to TMA, crystalline

alumium could not be produced. The data indicate that the ratio of H_2/TMA flows should be on the order of at least 60. A summary of the reported average crystallite sizes are shown in table 4.4.

Table 4.4: **Hydrogen study crystallite sizes**

Carrier Ar (sccm)	**Average crystallite size (Å)**
8	N/A
10	N/A
15	44
20	44

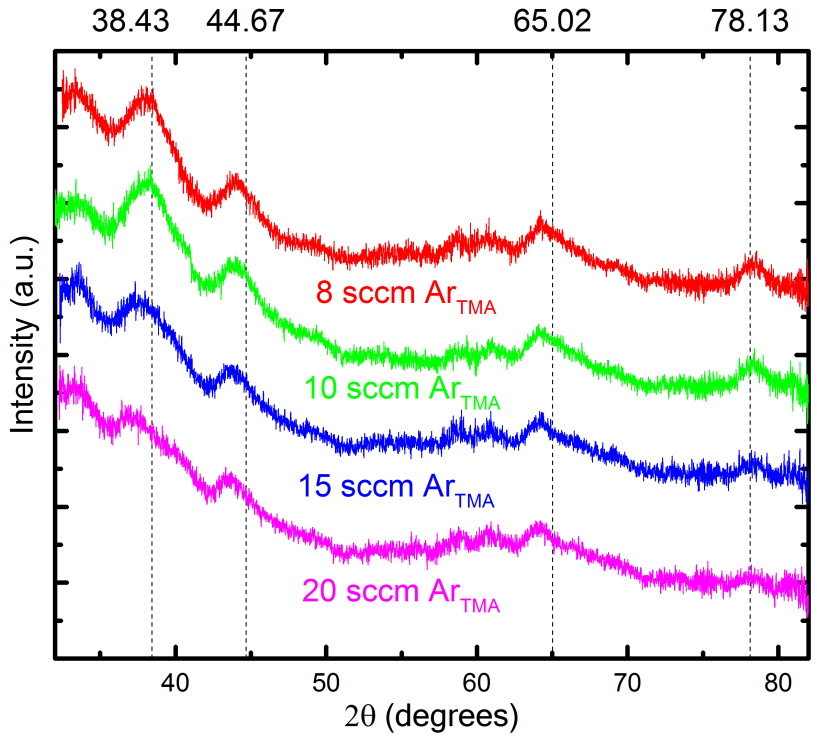

Figure 4.11: 30-min XRD data acquisitions of aluminum nanoparticles synthesized using 8-20 sccm carrier Ar in 15 W plasmas. The total flow rate used to produce each sample was 100 sccm. The H_2 flow rate was held constant at 80 sccm for all trials. The dilution argon flow rate was set to maintain a total flow rate of 100 sccm. As the TMA flow rate increased (with a corresponding decline in H_2/TMA) the crystallinity of the samples decreased. Dotted lines denote standard FCC elemental aluminum diffraction peaks.

Chapter 5

Conclusion and Discussion

A nonthermal plasma glow discharge containing TMA vapor, argon and hydrogen gases was capable of synthesizing nanoparticles containing crystalline aluminum. According to XPS analysis only 7% of aluminum atoms in the sample were occupied by elemental aluminum. The rest were present in the form of aluminum oxide Al_2O_3 or as hydroxide. XPS depth profiling showed that the amount of elemental aluminum in the sample was uniform. This suggests that the base pressure of the system was too high. Since aluminum is extremely sensitive to the presence of oxygen, just a small amount of air leakage into the reactor would be enough to form aluminum oxide while the nanoparticles grew in size.

A minimum amount of hydrogen flow (70% of the total Ar/TMA/H2 flow rate) was required to synthesize crystalline elemental aluminum. OES measurements of the plasma found that as the percentage of H_2 gas flow increased, the size of the H-α peak did as well. This positive trend provided a way to evaluate in-situ whether the plasma was indeed producing crystalline aluminum nanoparticles.

XRD characterization of air-free samples showed that the crystallite size of aluminum in the nanoparticles was smaller than what would be required to handle them in air. Since aluminum oxide shell thickness on a nanoparticle can be as large as 5 nm, the nanoparticles synthesized in the Ar/H_2/TMA plasma would need to be larger than 10 nm in diameter. Otherwise they would oxidize completely. One issue was that the base pressure of the reactor was likely not as low as required for aluminum synthesis. For example, at a minimum it should be a pressure of 10^{-6} Torr, considering other reactor

configuration that have been used to deposit Al films [1].

If the size of the nanoparticles could be increased significantly by varying conditions in the reactor so that their diameter were larger than 20 nm, an elemental crystalline core could remain intact upon slow exposure to air bled into the system. For example, nickel and iron nanoparticles synthesized in a DC atmospheric pressure microplasma could be varied in size by increasing the concentration of their precursors in the plasma [25]. A similar approach could be used with TMA vapor to increase the size of aluminum nanoparticles produced within the plasma.

Future studies of aluminum nanoparticle synthesis in a nonthermal plasma reactor could be performed in a reactor with a much lower base pressure, starting on the order of 10^{-6} Torr. In addition, the size of these metal nanoparticles could be tuned by increasing the flow rate of metal precursor so long as the percentage of H_2 gas flow with respect to the total flow is at least 70% while maintaining an H_2/TMA ratio of at least 60.

References

[1] Mark W. Knight, Nicholas S. King, Lifei Liu, Henry O. Everitt, Peter Nordlander, and Naomi J. Halas. Aluminum for plasmonics. 8(1):834–840.

[2] USGS minerals information: Commodity statistics and information https://minerals.usgs.gov/minerals/pubs/commodity/. (Accessed March 22, 2017).

[3] Babak Alinejad and Korosh Mahmoodi. A novel method for generating hydrogen by hydrolysis of highly activated aluminum nanoparticles in pure water. *International Journal of Hydrogen Energy*, 34(19):7934–7938, October 2009.

[4] Christopher E. Bunker, Marcus J. Smith, K. A. Shiral Fernando, Barbara A. Harruff, William K. Lewis, Joseph R. Gord, Elena A. Guliants, and Donald K. Phelps. Spontaneous Hydrogen Generation from Organic-Capped Al Nanoparticles and Water. *ACS Applied Materials & Interfaces*, 2(1):11–14, January 2010.

[5] Linan Zhou, Chao Zhang, Michael J. McClain, Alejandro Manjavacas, Caroline M. Krauter, Shu Tian, Felix Berg, Henry O. Everitt, Emily A. Carter, Peter Nordlander, and Naomi J. Halas. Aluminum Nanocrystals as a Plasmonic Photocatalyst for Hydrogen Dissociation. *Nano Letters*, 16(2):1478–1484, February 2016.

[6] Mark T. Swihart. Vapor-phase synthesis of nanoparticles. *Current Opinion in Colloid & Interface Science*, 8(1):127–133, 2003.

[7] W. Mahoney and R. P. Andres. Aerosol synthesis of nanoscale clusters using atmospheric arc evaporation. *Materials Science and Engineering: A*, 204(1-2):160–164, 1995.

[8] S. Schwyn, E. Garwin, and A. Schmidt-Ott. Aerosol generation by spark discharge. *Journal of Aerosol Science*, 19(5):639–642, 1988.

[9] Horst Hahn. Gas phase synthesis of nanocrystalline materials. *Nanostructured Materials*, 9(1-8):3–12, 1997.

[10] Toivo T. (Toivo Tarmo) Kodas and Mark J Hampden-Smith, editors. *The chemistry of Metal CVD*. Weinheim, Weinheim, 1994.

[11] Hamid Ghorbani. A Review of Methods for Synthesis of Al Nanoparticles. *Oriental Journal of Chemistry*, 30(4):1941–1949, December 2014.

[12] Dan A. Kaplowitz, R. J. Jouet, and Michael R. Zachariah. Aerosol synthesis and reactive behavior of faceted aluminum nanocrystals. *Journal of Crystal Growth*, 312(24):3625–3630, 2010.

[13] Bin Zhang. *Thermal plasma synthesis and photoinduced coating of aluminum nanoparticles*. Ph.D., University of Minnesota, Twin Cities, 2007. 3263150.

[14] Ashish. Rai. *Characterization and reactivity of aluminum nanoparticles*. PhD thesis, 2005.

[15] John C. Weigle, Claudia C. Luhrs, C. K. Chen, W. Lee Perry, Joseph T. Mang, Martin B. Nemer, Gabriel P. Lopez, and Jonathan Phillips. Generation of Aluminum Nanoparticles Using an Atmospheric Pressure Plasma Torch. *The Journal of Physical Chemistry B*, 108(48):18601–18607, December 2004.

[16] L. Zhang, M.B. Ranade, and J.W. Gentry. Formation of organic coating on ultrafine silver particles using a gas-phase process. *Journal of Aerosol Science*, 35(4):457–471, April 2004.

[17] Uwe R. Kortshagen, R. Mohan Sankaran, Rui N. Pereira, Steven L. Girshick, Jeslin J. Wu, and Eray S. Aydil. Nonthermal Plasma Synthesis of Nanocrystals: Fundamental Principles, Materials, and Applications. *Chemical Reviews*, 116(18):11061–11127, September 2016.

[18] NIST chemistry webbook. http://webbook.nist.gov/chemistry/.

[19] Masu Kazuya, Sakur Jun, Shigeeda Nobuyuki, Tsubouchi Kazuo, Mikoshiba Nobuo, and Takeuti Yosihisa. Aluminum Deposition from Weekly-Excited Metalorganic Source by Hybrid-Excitation CVD, 1988.

[20] Kazuya Masu, Kazuo Tsubouchi, Nobuyuki Shigeeda, Tatsuya Matano, and Nobuo Mikoshiba. Selective deposition of aluminum from selectively excited metalorganic source by the rf plasma. *Applied Physics Letters*, 56(16):1543, 1990.

[21] K Tsubouchi and K Masu. Precursor design and selective aluminum CVD. *Vacuum*, 46(11):1249–1253, November 1995.

[22] Takashi Kato, Takashi Ito, and Mamoru Maeda. Chemical Vapor Deposition of Aluminum Enhanced by MagnetronPlasma. *Journal of The Electrochemical Society*, 135(2):455–459, February 1988.

[23] M.A. Lieberman and A.J. Lichtenberg. *Principles of Plasma Discharges and Materials Processing: Second Edition*. 2005. DOI: 10.1002/0471724254.

[24] Yong-Chun Kim, Hyung-Ho Park, John S. Chun, and Won-Jong Lee. Compositional and structural analysis of aluminum oxide films prepared by plasma-enhanced chemical vapor deposition. *Thin Solid Films*, 237(1-2):57–65, 1994.

[25] Wei-Hung Chiang and R. Mohan Sankaran. Microplasma synthesis of metal nanoparticles for gas-phase studies of catalyzed carbon nanotube growth. *Applied Physics Letters*, 91(12):121503, September 2007.